Journal of the European Ceramic Society 37 (2017) 297–303

Contents lists available at www.sciencedirect.com

Journal of the European Ceramic Society

journal homepage: www.elsevier.com/locate/jeurceramsoc

Sliding wear of $CaZrO_3$-MgO composites against ZrO_2 and steel

Abílio Silva[a,b], Fernando Booth[a,c], Liliana Garrido[c], Esteban Aglietti[c], Pilar Pena[a], Carmen Baudín[a,*]

[a] Instituto de Cerámica y Vidrio, ICV-CSIC, Kelsen 5, Madrid 28049, Spain
[b] C-MAST, Department of Electromechanical Engineering, University of Beira Interior, 6200-001 Covilhã, Portugal
[c] CETMIC (Centro de Tecnología de Recursos Minerales y Cerámica, CIC-CONICET La Plata), Camino Centenario y 506, C.C.49 (B1897ZCA) M.B. Gonnet, Buenos Aires, Argentina

ARTICLE INFO

Article history:
Received 10 May 2016
Received in revised form 20 July 2016
Accepted 23 July 2016
Available online 1 August 2016

Keywords:
$CaZrO_3$
MgO
Abrasive wear
Adhesive wear
Pin-on-disc

ABSTRACT

The wear behaviour of a fine grained and dense $CaZrO_3$-MgO composite is presented. Un-lubricated Pin-on-disc tests at room temperature have been performed using 10 N as normal force and 0.10–0.15 ms^{-1} as sliding rate and ZrO_2 and steel counterparts. The coefficient of friction versus the sliding distance and the specific wear, together with a complete microstructural analysis of the worn surfaces by field emission scanning electron microscopy is reported. The composite presents a wear resistance similar to other ceramics under ceramic/ceramic sliding contact and improved wear resistance in contact with steel.

Initial wear is dominated by abrasion independently of the chemical nature of the counterpart. The second stage wear depends on the characteristics of the third body formed. Zirconia leads to a brittle particulate third body with little protective capability. Steel forms a strongly bonded and plastic cermet third body that protects the material limiting the level of further wear.

1. Introduction

Calcium zirconate ($CaZrO_3$) is a ceramic oxide of the perovskite family that presents several properties of interest as structural as well as functional material. [1–4] It is known as a ceramic material for high temperature applications due to its high melting point (~2365 °C) and excellent corrosion resistance against alkali, earth alkali oxides, and basic slags, in particular against KOH and mixtures of $NaVO_2$ and Na_2SO_4 environments. At low oxygen pressure $CaZrO_3$ is an oxygen ion conductor, whereas at high oxygen pressure it is a mixed ion and electronic conductor. Due to their high chemical stability and good ionic conductivity at elevated temperatures, $CaZrO_3$ materials are used in devices to monitor oxygen, hydrogen and water, such as oxygen sensors for steel melts and for solid oxide galvanic cells. $CaZrO_3$ has also considerable interest for fuel cells, filler, resonator for microwave telecommunication and temperature compensating materials of capacitance multilayer ceramic capacitors or dielectric applications because its displays a high dielectric permittivity, around 30, low dissipation factor, with a temperature coefficient of capacitance of 40 ppm $°C^{-1}$ and a good behaviour under electrical field versus temperature.

$CaZrO_3$ based materials are also alternative refractories for casting titanium and its alloys, because they have the advantage of being inert to hydration while showing similar performance in use as CaO [5,6].

MgO-$CaZrO_3$ composites have been suggested as chrome free refractories to replace not only magnesia – chromite, but also magnesia over saturated spinel refractories. First temperature for liquid formation in pure MgO-$CaZrO_3$ is 2060 °C and $CaZrO_3$ is compatible with the main phases of Portland cement clinker in the solid state (C_2S:Ca_2SiO_4, C_4AF:$Ca_4Al_2Fe_2O_{10}$ and C_3S:Ca_3SiO_5). Therefore, $CaZrO_3$ as a second phase of MgO refractories would improve their resistance against clinker phase melting and alkali attack. Moreover, $CaZrO_3$ increases the resistance of MgO to hydration and thermal shock [7–11].

In addition, due to the similarities between the thermal expansion and thermal conductivity of $CaZrO_3$ and Y_2O_3-fully stabilised ZrO_2 (YFSZ), $CaZrO_3$ has been proposed as potential candidate for thermal and environmental barrier coatings (TBC, EBC). [12,13].

Due to the above described characteristics, $CaZrO_3$ – based materials can be considered as a good alternative to YFSZ for structural applications [14].

* Corresponding author.
E-mail address: cbaudin@icv.csic.es (C. Baudín).

http://dx.doi.org/10.1016/j.jeurceramsoc.2016.07.029
0955-2219/

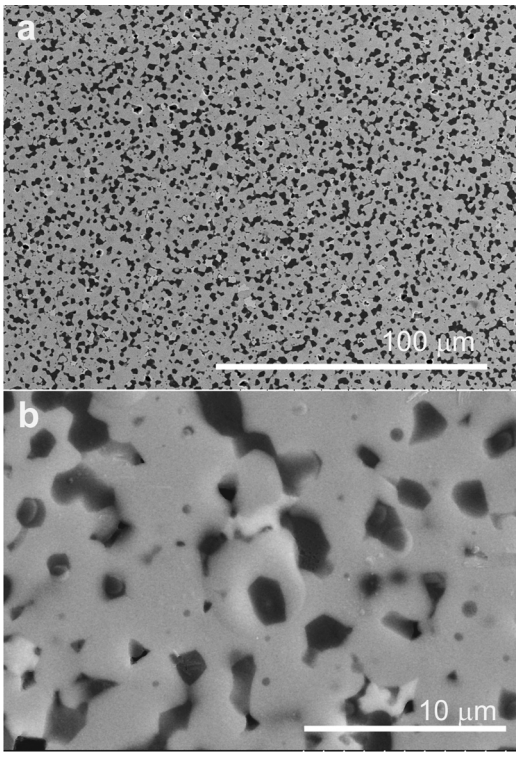

Fig. 1. Main microstructural features of the $CaZrO_3$- MgO studied composite, DBZ. The black areas with shinny borders are pores. Major phase (gray) is $CaZrO_3$ (EDX analysis, wt.%: ≈31–33 CaO and ≈67–69 ZrO_2) and the clearest particles are c-ZrO_2 (EDX analysis, wt.%: 2–4 MgO, 8–10 CaO and 85–89 ZrO_2). The second phase (black) is MgO.
(a) Low magnification SEM micrograph (BSE COMPO image).
(b) High magnification FE-SEM micrograph. Small amounts of glass (dark gray) are observed together with the MgO particles dispersed in the $CaZrO_3$ matrix.

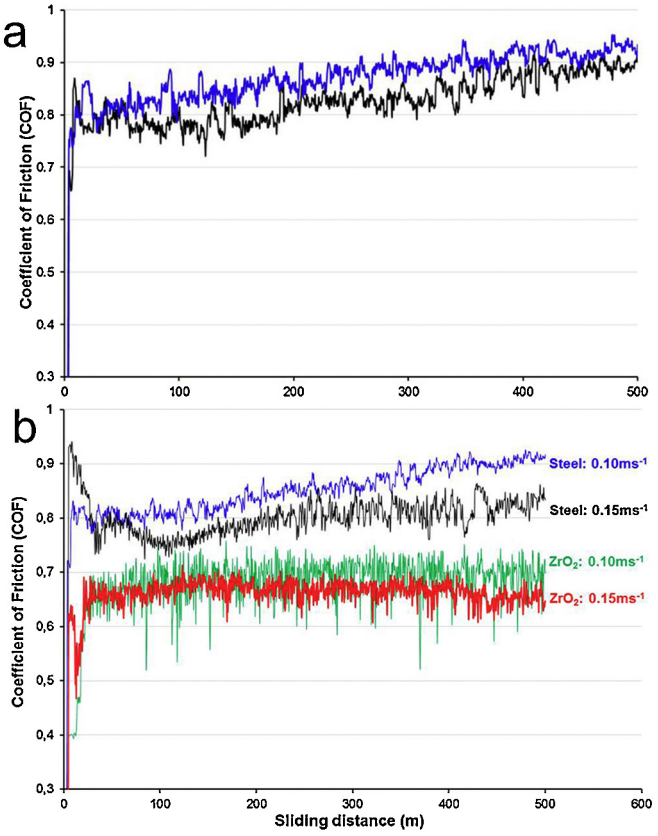

Fig. 2. Evolution of the coefficient of friction with the sliding distance.
(a) Values for two nominally identical tests.
(b) Average values for the four experimental conditions used.

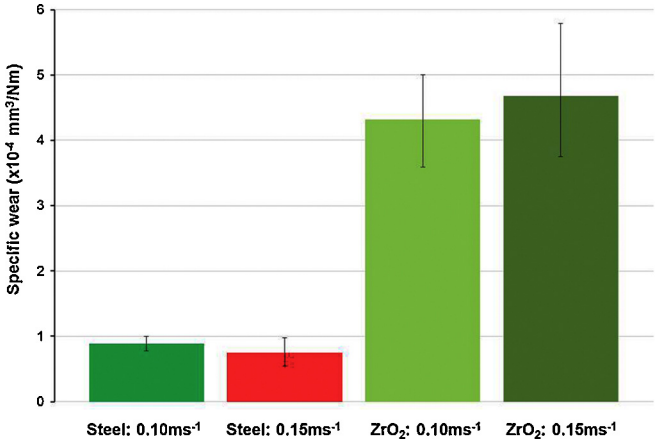

Fig. 3. Specific wear for the indicated experimental conditions.

$CaZrO_3$ is very rare in nature due to its high crystallization temperature and the high affinity of Zr with Si, resulting in the formation of $ZrSiO_4$ instead of $CaZrO_3$.

There are several methods to synthesize $CaZrO_3$, being the most used one the solid state reaction of equimolar CaO-ZrO_2 mixtures. The use of natural limestone or dolomite, with consistent chemical composition, mixed with ZrO_2 is an attractive alternative way for the low cost production of structural refractory materials.

shows the specific wear values. Differences between values for different tests under nominally equal experimental conditions were inside the variability limits of those obtained for one wear track. The volume loss for tests performed using ZrO_2 balls was significantly larger than for those performed with steel. There were no significant differences between values for different sliding rates.

The balls used as counterparts also lost some volume after testing, especially in the case of the ZrO_2 ones which presented elliptical wear scars as shown in Fig. 4

Particularly, composite materials $CaZrO_3$-MgO have been investigated as refractories for steel and cement industry [7–10,15].

In a previous work [14] it was demonstrated that fine grained and dense $CaZrO_3$-MgO based materials with potential uses in advanced structural applications can be fabricated from natural dolomites if the nature and amount of impurities is carefully controlled. In particular, the phase composition – mainly the presence and amount of c-ZrO_2 and glass as secondary phases- and the grain size of the sintered materials are highly dependent on impurities in the natural dolomites used. Higher glass content and larger microstructure were responsible for lower hardness and strength of the lowest purity material. Moreover, depending on the nature of the minor impurities, the silica liquids formed in these materials might present low viscosity at low temperature (≈1400 °C) which would restrain their use in structural applications of responsibility.

All of the above mentioned actual and potential applications of $CaZrO_3$-MgO based composites require the materials to be resistant to wear. Consequently, the study of their surface damage mechanisms when interacting with other surfaces is required.

This study is focused to understanding the sliding wear behaviour of $CaZrO_3$-MgO composites. From the previously developed materials, the one fabricated with the purest raw materials was chosen for this investigation. It is well known that the mechanical and chemical interactions of the contact surfaces remarkably

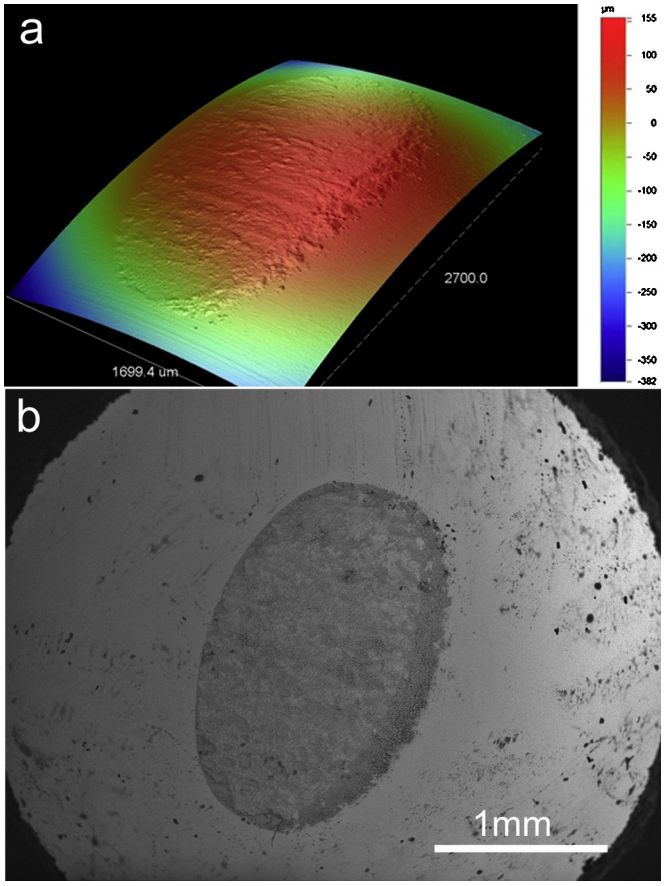

Fig. 4. Elliptical wear scar on the surface of a ZrO_2 ball after testing a sliding distance of 500 m at velocity of 0.1 ms^{-1}.
(a) Topographic image. The legend bar shows the relative depths associated to the different colours.
(b) SEM micrograph.

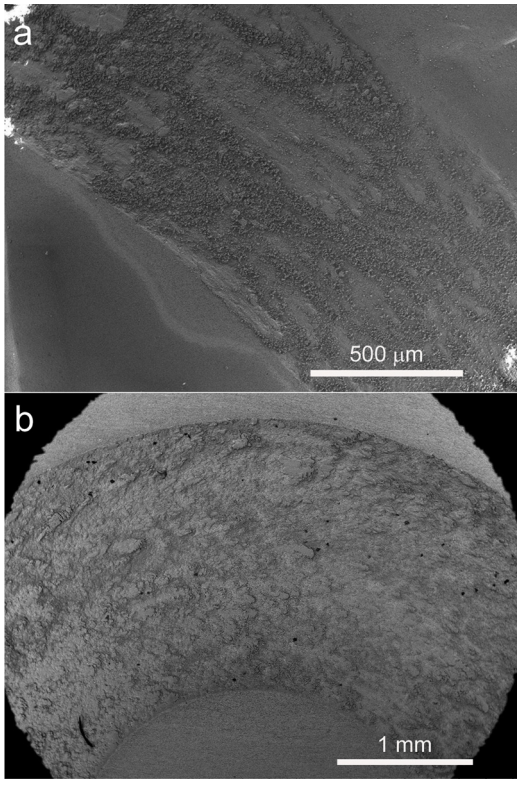

Fig. 5. Macroscopic aspect of the wear tracks. Characteristic low magnification SEM micrograph.
(a) Specimen tested using a stainless steel ball as counterpart.
(b) Specimen tested using a ZrO_2 ball as counterpart.

modify the tribological characteristics of ceramic couples. Therefore, counter bodies of two different natures were chosen for the study. The wear behavior at room temperature under un-lubricated conditions of two tribo pairs is described: (i) $CaZrO_3$-MgO composite against steel; (ii) $CaZrO_3$-MgO composite against zirconia. Zirconia has been chosen as ceramic counterpart due to the chemical compatibility with the studied composite.

2. Experimental

The complete characterisation of the raw materials and the detailed processing procedure are reported elsewhere [14]. The starting materials were a natural Argentinean dolomite $MgCa(CO_3)_2$ and a commercial high purity (99.9%) monoclinic zirconia, m-ZrO_2 with d_{50} = 0.44 μm (Saint Gobain – Zir Pro, China), mixed in proportion 1:1 mol. The dolomite (DB) consisted mainly of $MgCa(CO_3)_2$ and contained calcite as minor constituent; main impurities were Al_2O_3 (0.2 wt.%) and SiO_2 (1 wt.%).

The powders were attrition milled during 4 h with zirconia balls and using isopropyl alcohol as media. Final average particle size was, d_{50} = 0.60 μm. The milled powders were dried at 60 °C during 24 h and uniaxially pressed at 20 MPa into discs and sintered at 1450 °C during 2 h. Final sizes were ≈10 mm of diameter and ≈8 mm of thickness.

The surfaces to be subjected to sliding during the wear tests were diamond polished down to 3 μm, cleaned using ethanol and dried. The surface heights across five areas of 10 μm × 10 μm in the polished surfaces were recorded by atomic force microscope, AFM (Cervantes, Nanotec Electrónica, Spain) and the roughness of the of the surfaces was evaluate in terms of the Root Mean Square (RMS) values. Given values are the average of the five determinations and errors are the standard deviations.

Wear tests were performed on a disk tribometer (tribotester UMT-3, CETR, Bruker, USA). The counter bodies were balls of 6.3 mm diameter made of stainless steel 440 (~748 HV, MatWeb, material property data, www.matweb.com) and ZrO_2 ball, (~1300 HV, Hightech ceram Dr. Steinman, htc-YPSZ1, Germany).

All tests were performed at room temperature under a normal force (F) of 10 N at sliding speeds of 0.1 and 0.15 ms^{-1}. The track radius varied from 2 mm (0.1 ms^{-1}) to 5 mm (0.15 ms^{-1}), the frequency of contact was 7.96 Hz (0.1 ms^{-1}) and 4.77 Hz (for 0.15 ms^{-1}) and the total sliding distance (S) was equal to 500 m for all tests. During each test, the coefficient of friction (COF) was continuously recorded.

The microstructural characterization of the wear tracks was performed on Ag-coated specimens using a Field Emission Scanning Electron Microscope, FE-SEM, with analysis by energy dispersive X-ray spectroscopy (EDS) (Hitachi, S-4700 type I, Japan). Unless specifically indicated, all micrographs correspond to secondary electrons. Quantitative analyses were performed using the internal corrections of the equipment.

The volume of removed material was quantified using a contact perfilometer (Bruker Dektak XT) by scanning the surface perpendicular to the wear track. First, four 2D profiles of sections of the wear track at 0, 90, 180 and 270° were done and the average of the hollow surfaces of the four profiles was calculated. The total wear volume after testing was then calculated by multiplying this average by the circumference of the wear track, in agreement with the standard ASTM G99. The specific wear rates K were then calculated according to the following equation:

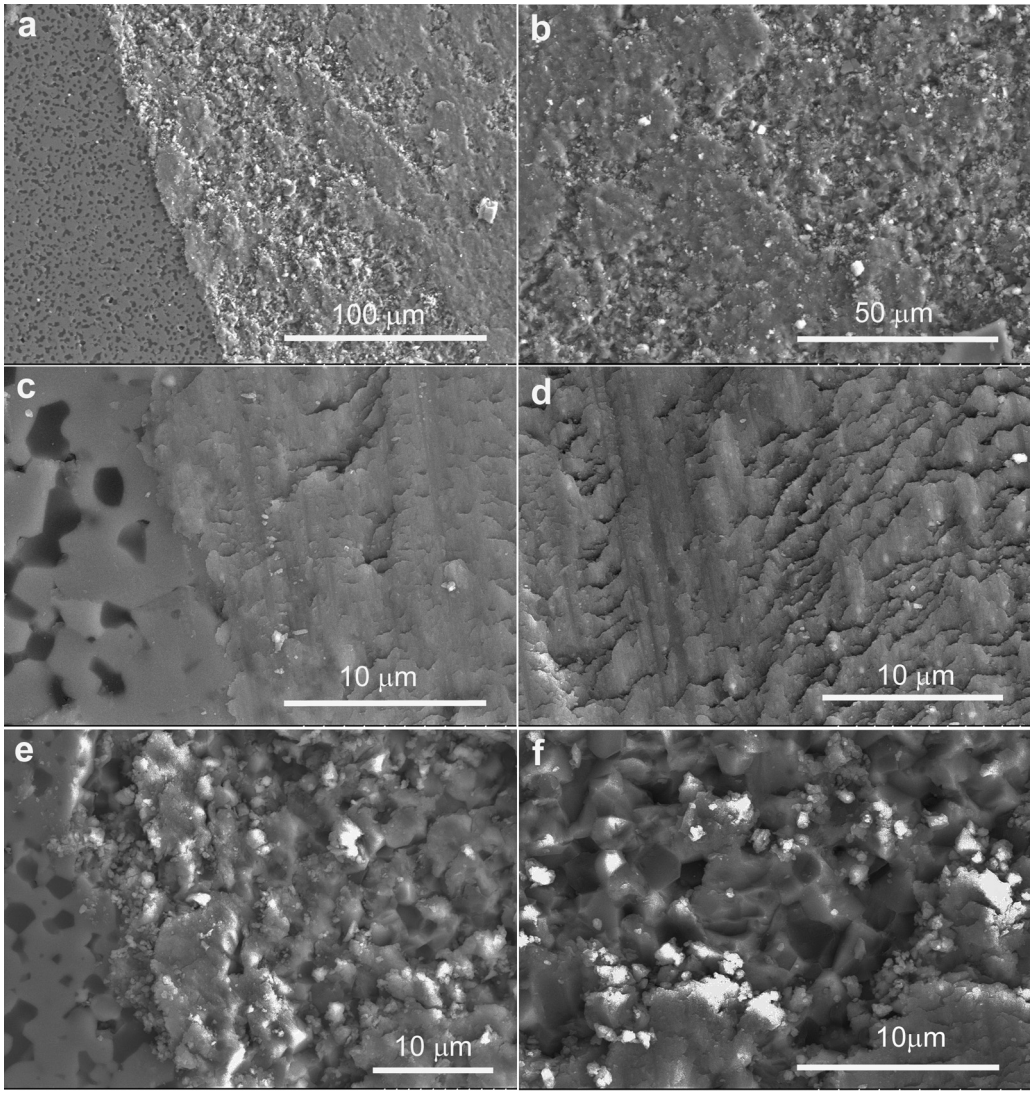

Fig. 6. Characteristic features of the wear tracks of specimens tested using stainless steel balls. (a), (c) and (e) correspond to the transition regions and (b), (d) and (f) to the central parts. FE-SEM micrographs.
(a) and (b): low magnification micrographs showing flat compacted surfaces and zones with un-compacted debris particles.
(c) and (d): details of (a) and (b), respectively, showing heavily smeared surfaces with abrasion grooves.
(e): detail of (a) showing numerous debris particles.
(f): detail of (b) showing a fractured surface. MgO (dark) and c-ZrO_2 (bright) grains present transgranular fracture and the $CaZrO_3$ matrix (bright) presents intergranular fracture.

$K = \frac{V}{F \cdot S}$ where V is the volume of removed material (mm^3), F the normal load (N) and S the sliding distance (m).

Topographic (3D) images of the worn areas of the balls were obtained using 2D profiles taken each 5 μm; a total of 540 profiles were used.

3. Results

The microstructural characteristics of the studied material, DBZ, are fully reported elsewhere [14]. Fig. 1 shows the main microstructural features of the material which was dense (≈100% T.D.) and homogeneous.

Major crystalline phases were $CaZrO_3$ (75.4 ± 0.5 wt.%) and MgO (18.8 ± 0.4 wt.%); c-ZrO_2 ($Ca_{0.15}Zr_{0.85}O_{1.85}$, 2.2 ± 0.1 wt.%) and merwinite ($Ca_3Mg(SiO_3)_2$, 3.7 ± 0.3 wt.%) were present as minor phases. Small glass pockets were observed (Fig. 1b) and 4 wt.% of non-diffracting phases was identified by Rietveld analysis.

The polished surfaces presented low and homogeneous roughness (Root Mean Square, RMS = 5.7 ± 0.2 nm).

Fig. 2 shows the evolution of the coefficient of friction (COF) with the sliding distance. Results for nominally identical tests were fairly coincident (Fig. 2a).

For the tests performed with ZrO_2 balls, the COF attained a constant value after a short running-in stage (≈70 m) with an initial (≈30 m) sharp decrease. Conversely, for the tests performed with steel balls, values increased continuously after the initial (≈50 m) decrease and no constant value was attained through the whole test. Values for the tests performed using steel were higher (≈0.8–0.9) and more variable than those obtained when ZrO_2 was used (≈0.6–0.7). In both cases, the COF was slightly higher for the lowest sliding rate used.

Fig. 3. Fig. 5 shows the general aspect the wear tracks formed in the tested specimens. All tracks presented a regular aspect with well-defined edges and symmetrical arches. Track widths for the specimens tested using the steel balls were about half of those formed when ZrO_2 balls were used.

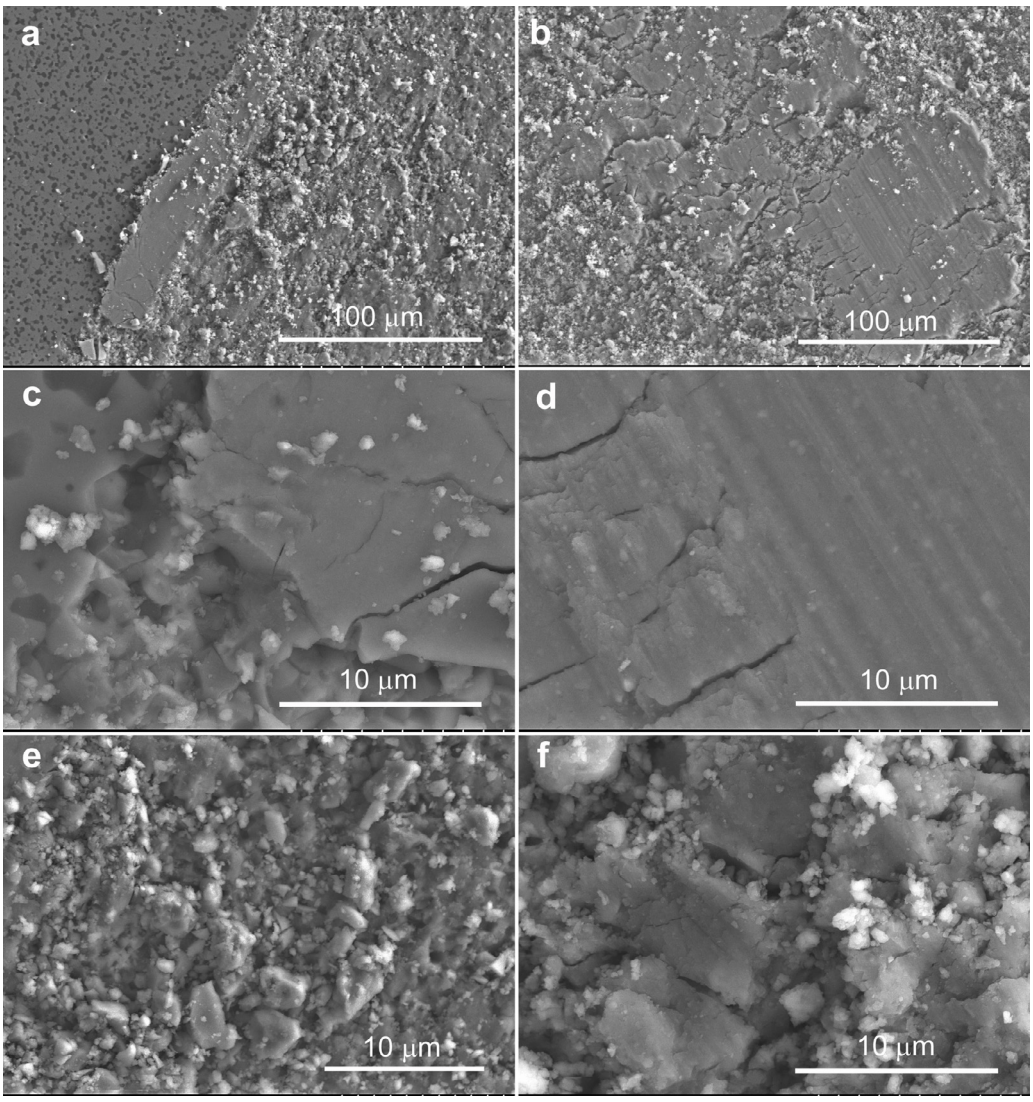

Fig. 7. Characteristic features of the wear tracks of specimens tested using ZrO_2 balls. (a), (c) and (e) correspond to the transition regions and (b), (d) and (f) to the central parts. FE-SEM micrographs.
(a) and (b): low magnification micrographs showing flat compacted surfaces and zones with un-compacted debris particles.
(c) and (d): details of (a) and (b), respectively, showing flat compacted surfaces with cracks and abrasion grooves.
(e): detail of (a) showing debris particles.
(f): detail of (b) showing debris particles and small compacted areas.

The characteristic microstructural features found in the wear tracks are summarized in Figs. 6 and 7. In order to understand the microstructural changes during the wear, the microstructure of the transition areas (borders of the tracks) was analysed separately from that of the central (interior) parts. The interior and exterior borders presented similar features. No differences were found between the microstructural features as a function of the sliding rate.

Both regions of the tracks, transition and central, formed in the specimens tested using steel balls presented flat compacted surfaces and zones with un-compacted debris particles at low magnification (Fig. 6a,b). Higher magnification of the flat areas revealed heavily smeared surfaces with abrasion grooves (Fig. 6c,d). The only differences between the two regions of the tracks formed in these specimens were found in the un-compacted zones. Details of the transition areas (Fig. 6e) revealed numerous debris particles and practically no original material was observed. In the central parts of the tracks, large portions of fractured original material were clearly observed (Fig. 6f). MgO grains presented transgranular fracture while the $CaZrO_3$ matrix presented intergranular fracture.

As in the case of specimens tested with steel balls, both regions of the tracks formed in the specimens tested using zirconia balls presented flat compacted surfaces and zones with un-compacted debris particles at low magnification (Fig. 7a,b). The compacted surfaces, which covered the major part of the tracks, presented cracks perpendicular to the sliding direction (Fig. 7c,d) and some abrasion grooves. In both regions, large zones of debris particles were found (Fig. 7e,f), with small compacted areas between them in the central regions of the tracks (Fig. 7f).

EDX analyses of the different zones showed that the relative amounts of material components in the different zones of the wear tracks of the specimens tested using both kinds of balls (wt.%: 16–22 of MgO, 25–28 of CaO and 50–58 of ZrO_2) were similar to those of the original material determined by chemical analysis (X-ray fluorescence wt.%: 18.0 of MgO, 26.1 of CaO and 54.7 of ZrO_2) [14]. In the specimens tested using steel, significant amounts of Fe were

detected in the tracks, especially in the compacted areas, as plotted in Fig. 8.

4. Discussion

The specific wear and COF values obtained in this work for the specimens tested using ZrO_2 balls are in the range of those reported for other structural ceramics tested using ceramic counter parts. In particular, similar values (specific wear $\approx 10^{-3}$–10^{-4} mm^3/Nm, COF $\approx$ 0.55–0.65) were obtained for Y_2O_3-stabilised ZrO_2 materials tested using ZrO_2 balls and nominally the same experimental conditions as in this work [16].

The high specific wear values ($\approx$10–4 mm^3/Nm, Fig. 3) reached by the specimens tested using both kinds of balls correspond to the occurrence of severe wear related to mechanical based mechanisms such as fracture. In fact, debris particles and detached grains were present in the wear tracks of all specimens (Figs. 6 and 7). However, most part of the wear tracks was constituted by compacted layers with grooves and no large cavities were observed in the tracks, which would correspond to the mild wear stage [17,18].

The heavily smeared surfaces of the compacted layers in the specimens tested using steel balls reveal the ductile character of the formed third body. Moreover, significant amounts of metal were transferred from the steel counterpart to the worn surface (Fig. 8). Taking into account the above facts, the wear mechanism of the studied material under sliding contact with steel can be described as follows. In the initial stages, brittle fracture and particle detachment occurred due to the nucleation and growth of microcracks originated by the cyclic stresses developed during the wear tests, increasing surface roughness. This would lead to a decrease of the friction coefficient due to the reduction of the real contact area and to a large value of the specific wear, as observed (Figs. 2 and 3) [19,20]. As the test proceeded, the fractured particles decreased their size to the submicrometric range (Fig. 6e,f) and adhesion between the steel ball and the material occurred by direct chemical reaction between the steel and the ceramic components, as observed for zirconia ceramics [21,22].

In general, adhesive wear occurs when the two contact surfaces have a high mutual chemical compatibility [23]. Friction between the specimen and the ball during testing leads to significant temperature increase in the contact region. Therefore, solid state reactions producing the formation of solid solutions of Fe in ZrO_2 and/or in MgO might take place during testing. In the system ZrO_2-FeO-Fe, levels of solid solution of FeO in ZrO_2 up to $\approx$5 mol% are expected at temperatures $\leq$1200 °C. [24] In the Fe—Mg—O system, the solid solutions of Fe in MgO might also be elevated at relatively low temperatures (T $\approx$ 1160 °C) [25].

The ductile third body formed in the composite material-steel system by the above described reaction filled the cavities formed due to the initial severe wear and the COF increased due to the smoother surface formed (Fig. 2). Then, damage of the material entered a second wear stage controlled by tribochemical mechanisms. In this stage, wear would be determined by the interaction between the steel ball and the cermet third body. The sudden jumps in the COF would correspond to the failure of highly deformed parts of the third body coating strongly adhered to the material that led to the show up of the newly fractured material surfaces (Fig. 6f).

The aspect of the compacted layers in the specimens tested using ZrO_2 balls, without smeared surfaces (Fig. 7a–d), reveals that they do not have an amorphous character as the tribofilms formed by the reaction of debris particles with moisture in other ceramics such as alumina [17]. The initial wear mechanism of the studied material under the effect of ZrO_2 counter parts was similar to that experienced when tested using steel balls. Brittle fracture and particle detachment that increased surface roughness and led to the observed decrease of the COF were the main processes. As the test proceeded, the fractured particles decreased their size to the submicrometric range (Fig. 7e,f) and mechanically mixed with some particles detached from the ball, to form a fine grained third body that filled the cavities formed due to the initial severe wear, compacting under the applied forces. During this processes, the COF increased due to the smoother surface formed and remained stable once this initial process finished (Fig. 2).

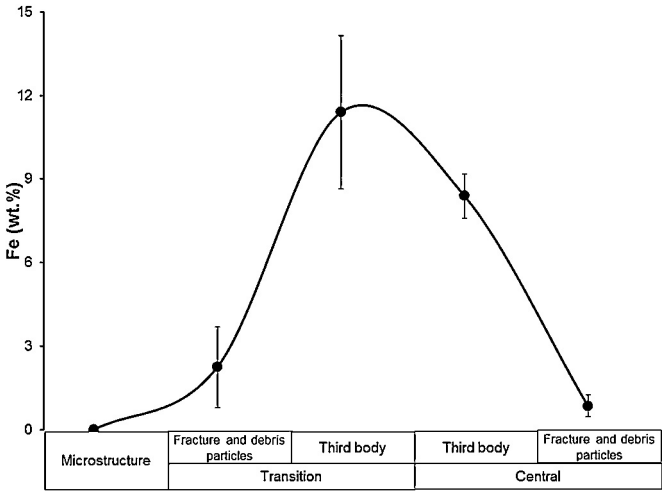

Fig. 8. Amount of Fe in the different regions of the wear tracks in specimens tested using steel balls.

Once the third body was formed and compacted, further surface damage was determined by the interaction of the third body with the ZrO_2 counterparts. The tensile stresses developed at the trailing edge of the contact areas originated the observed abrasion grooves and cone cracks (Fig. 7b–d). This second stage was mainly mild wear and the small occasional variances in the COF plots can be attributed to the pull out of parts of the third body. As there was not adhesion by chemical reaction between the third body and the worn material, the surfaces that showed up when the third body was detached were debris particles and worn material, and no fracture surfaces were revealed as occurred in the case of the steel balls (Fig. 7f).

5. Conclusions

The studied $CaZrO_3$-MgO composite presents a wear resistance similar to other ceramics under similar conditions of ceramic/ceramic sliding contact and improved wear resistance in contact with steel.

Initial wear is dominated by abrasion-fracture and detachment of particles- independently of the chemical nature of the counterpart. The second stage wear is dependent on the characteristics of the third body formed, which are determined by the chemical affinity between the material and the counterpart.

In the case of the compatible zirconia counterpart, a compacted particulate third body that physically fills the cavities and whose detachment reveals non-fractured material is formed. This loosely bonded and brittle third body has very little protective capability.

In the case of the non-compatible steel counterpart, a cermet third body that fills the cavities by adhesion to the material and whose detachment reveals fractured material is formed.

This strongly bonded and plastic third body protects the material and limits the level of further wear.

Acknowledgements

This work has been performed in the frame of the CYTED network 312RT0453 (HOREF, Spain) and supported by the Spanish Government under project MAT2013-48426-C2-1-R.

Abilio Silva acknowledges the support from the Portuguese national funding agency FCT-Fundação para a Ciência e a Tecnologia through the grant: SFRH/BSAB/105760/2014, the financial support of JECS Trust through mobility Contract 2015 97 and Instituto de Cerámica y Vidrio-CSIC.

References

[1] S. Schafföner, C.G. Aneziris, H. Berek, J. Hubálková, A. Priese, Fused calcium zirconate for refractory applications, J. Eur. Ceram. Soc. 33 (15–16) (2013) 3411–3418.
[2] W.J. Lee, A. Wakahara, B.H. Kim, Decreasing of $CaZrO_3$ sintering temperature with glass frit addition, Ceram. Int. 31 (4) (2005) 521–524.
[3] S.C. Hwang, G.M. Choi, The mixed ionic and electronic conductivity of $CaZrO_3$ with cation nonstoichiometry and oxygen partial pressure, Solid State Ionics 179 (21–26) (2008) 1042–1045.
[4] M. Dudek, E. Drozdz-Ciesla, Some observations on synthesis and electrolytic properties of nonstoichiometric calcium zirconate, J. Alloys Compd. 475 (2009) 846–854.
[5] M.G. Kim, S.K. Kim, Y.J. Kim, Effect of mold material and binder on metal-mold-interfacial reaction for investment castings of titanium alloys, Mater. Trans. JIM 43 (4) (2002) 745–750.
[6] C. Yuan, X. Cheng, P.A. Withey, Investigation into the use of $CaZrO_3$ as a face coat material in the investment casting of TiAl alloys, Mater. Chem. Phys. 155 (2015) 205–210.
[7] S. Serena, M.A. Sainz, A. Caballero, The system Clinker-MgO-$CaZrO_3$ and its-application to the corrosion behavior of $CaZrO_3$/MgO refractory matrix by clinker, J. Eur. Ceram. Soc. 29 (11) (2009) 2199–2209.
[8] J. Szczerba, Z. Pedzich, The effect of natural dolomite admixtures on calcium zirconate-periclase materials microstructure evolution, Ceram. Int. 36 (2) (2010) 535–547.
[9] J.L. Rodríguez, P. Pena, Obtención de materiales de magnesia – circonato cálcico – silicato dicálcico por sinterización reactiva de mezclas de dolomita – circón. Estudio del procesamiento, Bol. Soc. Esp. Ceram. Vidrio 40 (6) (2001) 461–469.
[10] E.A. Rodríguez, G.A. Castillo, T.K. Das, R. Puente-Ornelas, Y. González, A.M. Arato, J.A. Aguilar-Martínez, $MgAl_2O_4$ spinel as an effective ceramic bonding in a MgO-$CaZrO_3$ refractory, J. Eur. Ceram. Soc. 33 (13–14) (2013) 2767–2774.
[11] A. Obregón, J.L. Rodríguez-Galicia, J. López-Cuevas, P. Pena, C. Baudín, MgO-$CaZrO_3$-based refractories for cement kilns, J. Eur. Ceram. Soc. 31 (1–2) (2011) 61–74.
[12] C. Cano, M.I. Osendi, M. Belmonte, P. Miranzo, Effect of the type of flame on the microstructure of $CaZrO_3$ combustion flame sprayed coatings, Surf. Coat. Tech. 201 (2006) 3307–3313.
[13] M. Belmonte, Advanced ceramic materials for high temperature applications, Adv. Eng Mater. 8 (8) (2006) 693–703.
[14] F. Booth, L. Garrido, E. Aglietti, A. Silva, P. Pena, C. Baudín, $CaZrO_3$-MgO structural ceramics obtained by reaction sintering of dolomite-zirconia mixtures, J. Eur. Ceram. Soc. 36 (2016) 2611–2626 http://dx.doi.org/10.1016/j.jeurceramsoc.2016.03.027.
[15] J.L. Rodriguez, C. Baudín, P. Pena, Relationships between phase constitution and mechanical behaviour in MgO-$CaZrO_3$-calcium silicate materials, J. Eur. Ceram. Soc. 24 (4) (2004) 669–679.
[16] M.S. Suh, Y.H. Chae, S.S. Kim, Friction and wear behavior of structural ceramics sliding against zirconia, Wear 264 (2008) 800–806.
[17] C. Baudín, A. Tricoteaux, H. Joire, Improved resistance of alumina to mild wear by aluminium titanate additions, J. Eur. Ceram. Soc. 34 (2014) 69–80.
[18] O. Borrero-López, A.L. Ortiz, A.D. Gledhill, F. Guiberteau, T. Mrozc, L.M. Goldmanc, N.P. Padture, Microstructural effects on the sliding wear of transparent magnesium-aluminate spinel, J. Eur. Ceram. Soc. 32 (2012) 3143–3149.
[19] M. Sedlacek, B. Podgornik, J. Vizintin, Influence of surface preparation on roughness parameters, friction and wear, Wear 266 (2009) 482–487.
[20] K.J. Kubiak, T.W. Liskiewicz, T.G. Mathia, Surface morphology in engineering applications: influence of roughness on sliding and wear in dry fretting, Tribol. Int. 44 (2011) 1427–1432.
[21] M. Hua, X. Wei, J. Li, Friction and wear behavior of SUS 304 austenitic stainless steel against Al_2O_3 ceramic ball under relative high load, Wear 265 (2008) 799–810.
[22] W.M. Rainforth, The sliding wear of ceramics, Ceram. Int. 22 (1996) 365–372.
[23] C.X. Li, J. Xia, H. Dong, Sliding wear of TiAl intermetallics against steel and ceramics of Al_2O_3, Si_3N_4 and WC/Co, Wear 261 (2006) 693–701.
[24] O. Fabrichnaya, D.P. Vlyuchkov, Assessment of experimental data and thermodynamic modeling in the Zr—Fe—O System, Metall. Mater. Trans. A 47 (2016) 152.
[25] I.H. Jung, S. Decterov, A.D. Pelton, Thermodynamic modelling of the Fe—Mg—O system, J. Phys. Chem. Solids 65 (2004) 1683–1695.